A Multimodal Feedback Sensing System for An Endovascular Surgery Robot

Xinming Li, *Member, IEEE*. Shuxiang Guo, *Fellow, IEEE*. Masahiko Kawanishi, and Keisuke Suzuki

***Abstract*—Robot-assisted endovascular surgery (RES) acts as a promising alternative to aid medical cures. To overcome the current limitations of single feedback sensing for surgeons in RES, in this work, a multimodal feedback sensing system integrated with four kinds of feedback (temperature, vibration, haptic, and vision) are developed, fabricated, and tested to provide immersive feedback sensing to surgeons, improve the transparency and safety for operations. A small-sized wearable sensing bracelet (WSB), assembled by Peltier module, vibration motor, and film thermistor, is designed to generate continuous real-time feedback sensing (thermal feedback and vibrating feedback) and measure the temperature of thermal feedback. The haptic interface can offer force feedback. The monitor window is able to provide visual feedback. Besides, a multilevel control strategy for the feedback sensing system is proposed to indicate different surgical conditions. The performance evaluation for three feedback and insertions (in vitro experiments) are carried out to verify the feasibility and repeatability. Insertion results by five subjects demonstrate that proposed multimodal feedback sensing system achieves fast response, immersive feedback, and large repetition capacity. Moreover, benefiting from the inspiration of multimodal feedback sensing, it is suitable to combine more feedback stimulus, even possible to explore newly immersive/spatial feedback sensing for leader-follower robotics.**

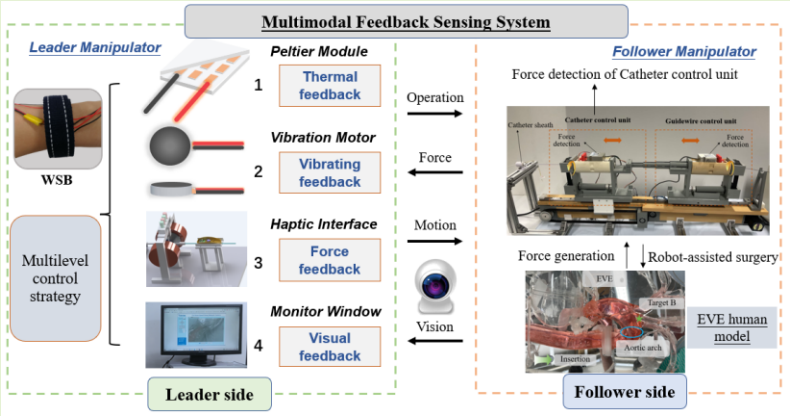

***Index Terms*—Multimodal feedback sensing, Endovascular surgery robot, Wearable sensing bracelet, Multilevel control strategy.**

I. Introduction

ROBOT-ASSISTED endovascular surgery (RES) has become one of the hot topics of research and is expected to be an ideal tool for medical application benefited from its significant advantages including surgical precision, operating comfort, avoiding radiation, minimally invasive, and good repeatability [1]-[2]. In RESs, the leader-follower robotic configurations are used for surgical teleoperations. The surgeon operates the leader device on the leader side and the robot replicates surgeon's operations on follower side. Meanwhile, to compensate the lack of feedback sensing for remote operations, force feedback, tactile feedback and visual feedback have emerged into robotic systems [3] since these feedback sensing directly relate to the transparency and safety of RES. Aiming to simulate the surgeon's operation as much as possible on leader side, operator's primary experience is based on the traditional feedback (force feedback and visual feedback). Tactile feedback (the characteristics for tactile sensing can be properties such as temperature, vibration, softness, texture, shape, composition, and shear [4]) is rarely mentioned in the field of RES but is frequently discussed in other fields [5]. Therefore, these types of researched feedback are entirely necessary to enhance the transparency and safety of operations.

For related research about force feedback. Various academics have been devoted to the implementations of force feedback, i.e., active, semi-active, and passive [6]. The active method generally needs designing a controllable force/torque

This work was supported in part by the Shenzhen "Medical Engineering Integration" Special Support Program Project under Grant F-2024-Z99-502365, Shenzhen, China; in part by the High level of special funds from Southern University of Science and Technology under Grant G03034K003, Shenzhen, China.

Corresponding author: Shuxiang Guo.

Xinming Li is with the School of Intelligent Manufacturing, Guangzhou Maritime University, Guangdong 510725, China, and also with the Graduate School of Engineering, Kagawa University, 2217-20 Hayashi-cho, Takamatsu, Kagawa 761-0396, Japan(e-mail: lixinming@gzmtu.edu.cn).

Shuxiang Guo is with the Department of Electric and Electrical Engineering, South University of Science and Technology, Guangdong 518055, China, and also with the Ministry of Industry and Information Technology, Beijing Institute of Technology, Beijing 100081, China (e-mail: guo.shuxiang@sustech.edu.cn).

Masahiko Kawanishi is with the Department of Neurological Surgery, Kagawa University, Takamatsu 761-0793, Japan (e-mail: mk@med.kagawa-u.ac.jp).

Keisuke Suzuki is with the Graduate School of Engineering, Kagawa University, 2217-20 Hayashi-cho, Takamatsu, Kagawa 761-0396, Japan (e-mails: suzuki.keisuke@kagawa-u.ac.jp).

generating structure, e.g., a linear motor [7] or series elastic actuator (SEA) [8] by the continuous control of applied current. Although active approach can offer fast dynamic response, it may lead to instability force capacity and additional resistance. For semi-active haptic method, the emerging smart materials, e.g., magnetorheological (MR) fluids [9] and magnetorheological (MR) elastomers [10], are used and assembled through controllable mechanical container as a cross-field solution. However, occasionally, these smart materials might generate inappropriate force according to the viscosity of magnetic materials [11]. As an adjustable and direct way, passive force feedback is normally employed to satisfy required force/torque by the control of friction resistant [12]. While it is a pretty stable and simple way to use, the dynamic bandwidth is limited by physical property and workspace of frictional contact surface [13]. Obviously, these efforts just can generate single feedback (force) and do not consider immersive sensing for surgeons. Considering a few special situations like surgeon's hand sensing has different sensitivity (caused by individual variations, surgical fatigue from constant work or differences in age), single feedback cannot make safe operations and multimodal feedback for surgeons, even might increase the risk of vascular rupture [14]. Few studies have done some attempts to improve transparency and safety operations [15]. However, for surgeon's sensing, these efforts only propose multimodal way to distinct force feedback with fixed safety threshold and set the magnifying factor based on surgical situations, which is not enough when figure's sensitivity has no big vary or force feedback embraces unknown troubles. Consequently, designing and exploring multimodal feedback sensing system that can offer integrated haptic sensing through various feedback would let RESs safer and more effective for both patients and surgeons.

For multimodal feedback sensing, the smart wrist-worn device (like bracelet) [16] has attracted explorations thanks to its advantages, e.g., small size, constant-available feedback, wearability. Benefiting from wrist-worn device, it becomes possible to explore multimodal feedback sensing (like vibration and temperature, both belong to tactile feedback [3]) through the cutaneous sense of surgeon's wrist [17]. Recent related research about bracelets has done a few attempts on composite sensors [18] and matrix arrangements [19] of vibration feedback. These works indicate that the wrist has a high sensitivity for both vibration and thermal feedback. Hence, wrist-worn devices also has potential applications for providing feedback sensing in RES.

In our prior effort, an endovascular robotic system [1] composed of collaborative handles and magnetically controlled haptic interface was proposed. This haptic interface can generate force sensing to surgeons by a magnetically controlled hydrogel (MCH), belongs to semi-active haptic method, but unable to offer immersive feedback sensing and improve the issue of sensing fatigue for long-time operation. Besides, in [1], key performance evaluations (like accuracy, resolution, response bandwidth) of proposed force feedback are loss. In [20], we did a number of studies for tremor suppression to ensure safe operation when conducting robot-assisted surgery. Consequently, in this work, to explore immersive feedback sensing, expand our previous research, and conduct performance evaluations for feedback perception, a multimodal feedback sensing system was proposed for VRS. The main contributions of this work are summaries as follows.

(1) A multimodal feedback sensing system integrated with four kinds of feedback (temperature, vibration, haptic, and vision) are developed, fabricated to provide immersive feedback sensing. Specifically, a small-sized WSB integrated vibration feedback and thermal feedback can easily generate continuous feedback sensing and measure the temperature of thermal feedback on surgeon's wrist.

(2) A flexible multilevel control strategy for the overall multimodal feedback sensing system was proposed to reconstruct immersive feedback sensing. It can improve the feedback sensing for surgeons to handle different surgical conditions based on four kinds of feedback sensing (temperature, vibration, haptic, and vision).

(3) A series of performance evaluation experiments for the proposed multimodal feedback sensing system were conducted including thermal, vibration, force and insertion performance (in vitro experiments). These experiments demonstrate that proposed feedback sensing systems can improve the safety and transparency of operations.

The remainder of this paper is organized as below. Clinical requirements are presented in Section II. Section III describes the proposed multimodal feedback sensing system, the developed endovascular surgery robotic, and control strategy. A series of performance evaluation experiments are introduced in Section IV. Finally, the conclusion is drawn in Section V.

II. Clinical Requirements

The concept diagram of the developed robot-assisted endovascular surgery is shown in Fig. 1, which mainly consisted of a leader manipulator, a follower manipulator, and the integrated WSB (offer vibration feedback and thermal feedback). Surgeons offer operational data via operating the leader manipulator (located in control room). The follower manipulator (located in operating room) conducts practical robot-assisted surgery after receiving motion command. Force feedback and visual feedback can be provided in real time as traditional feedback methods.

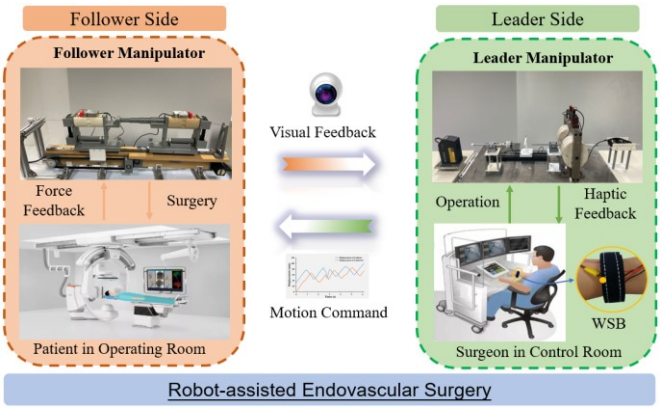

Fig.1. The concept diagram of the developed robot-assisted endovascular surgery.

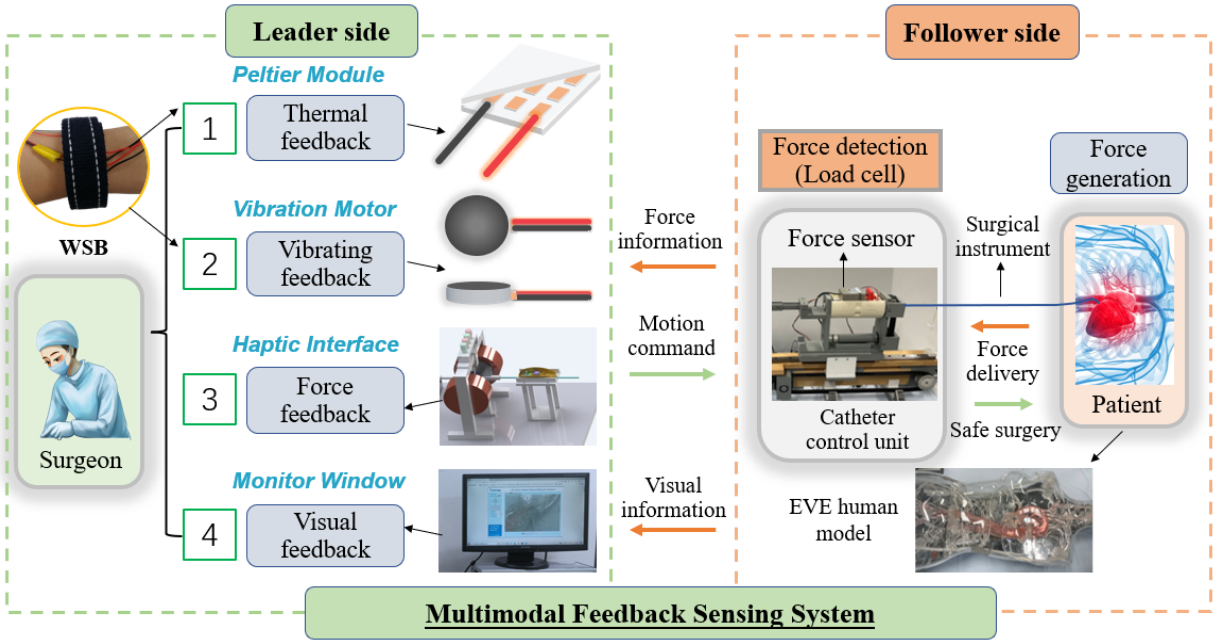

Fig.2. The proposed multimodal feedback sensing system.

Introducing the clinical requirements [21] of proposed multimodal feedback sensing system is significant to show the relevant performance needs for feedback sensing. As the visual feedback is a common approach for RES, we mainly discussed the other three feedback (thermal, vibration, and tactile). For thermal feedback sensing, [22] point out that, people can perceive a difference 0.03-0.09 °C of two warming pulses delivered to the hand. [23] indicate that the temperature sensor at the frequency of 5 Hz has the maximum bending strain. For vibration feedback, it demonstrates that the resolution of human's skin is 0.06 N [21], which could be used for both vibration (also as a form of force stimulus) and force feedback. [24] show that the stable frequency band of the vibration sensor is 5 to 170 Hz. As for force feedback, [25] point out that the magnetorheological actuator has a bandwidth of approximately 20 Hz enough high for force control. [21] indicate that the operating force generally not exceed 3.2 N. In addition, based on investigation with surgeon at hospital, acceptable sensing and clinical requirements for multimodal feedback sensing are determined as following:

(1) provide thermal feedback with a resolution less than 0.09 °C and a bandwidth of 5 Hz.

(2) generate vibration feedback with a resolution less than 0.06 N and a bandwidth in a range of 5 to 170 Hz.

(3) generate force feedback in a range of 3.2 N with a resolution of 0.06 N, and a bandwidth of roughly 20 Hz.

III. Feedback Sensing System and Control Strategy

The endovascular robotic system is a separate leader-follower solution to assist surgeons in practice. Generally, VIS robotic systems ought to satisfy three kinds of commands [26] including 1) leader manipulator can capture physician 's operation data and retain the surgical skills for safer operations of RES; 2) follower manipulator has ability to replicate surgeon's operation (e.g., for both catheter and guidewire) with high accuracy and fast response; 3) robotic system is possible to provide flexible, safer, and effective feedback sensing to operators based on immersive tactile sensation. Inspired by these concerns, multimodal feedback sensing is concepted and designed to offer an immersive feedback sensing for safe operation.

A. Multimodal Feedback Sensing System

To overcome shortage of single sensing approach (described in Section I), a multimodal feedback sensing system is designed based on a self-designed WSB, haptic interface, and monitor window. Both thermal feedback and vibrating feedback are integrated at the WSB for RES. The proposed feedback sensing system is shown in Fig. 2, which is an integrated sensing configuration for surgeons when conducting a surgery. The force detection is conducted by Load cell on follower side. More specifically, four sorts of feedback (thermal, vibration, haptic and visual) are employed to offer immersive sensing based on force information and visual information captured on follower side. Peltier module is able to offer fast response for the tasks of varying temperature as core thermal actuator in our study. Mini-type vibration motor is utilized to warn the safety of surgical procedures in real time. Benefiting from this system, actual surgical conditions with different blood vessels would be diversified reflected to surgeon's operation as safer guidance for RES. Moreover, multimodal feedback sensing can be used to improve the safety operation and reduce clinical training costs for interventionalists with different surgical experience (e.g., beginner, few experience, experienced).

B. Robotic System Configurations

1) **Wearable Sensing Bracelet (WSB)**

To build an immersive feedback sensing for operators when conducting RES, a WSB is designed and assembled for the robotic system with easily wearable and controllable advantages. Fig. 3 describes the elaborate assembly of WSB and instructions of relevant elements. The fabric-made wristband is bonded by Velcro. A Mini-type vibration motor (flattened vibrator, RB-See-403, 3.0V DC, Japan) is installed to

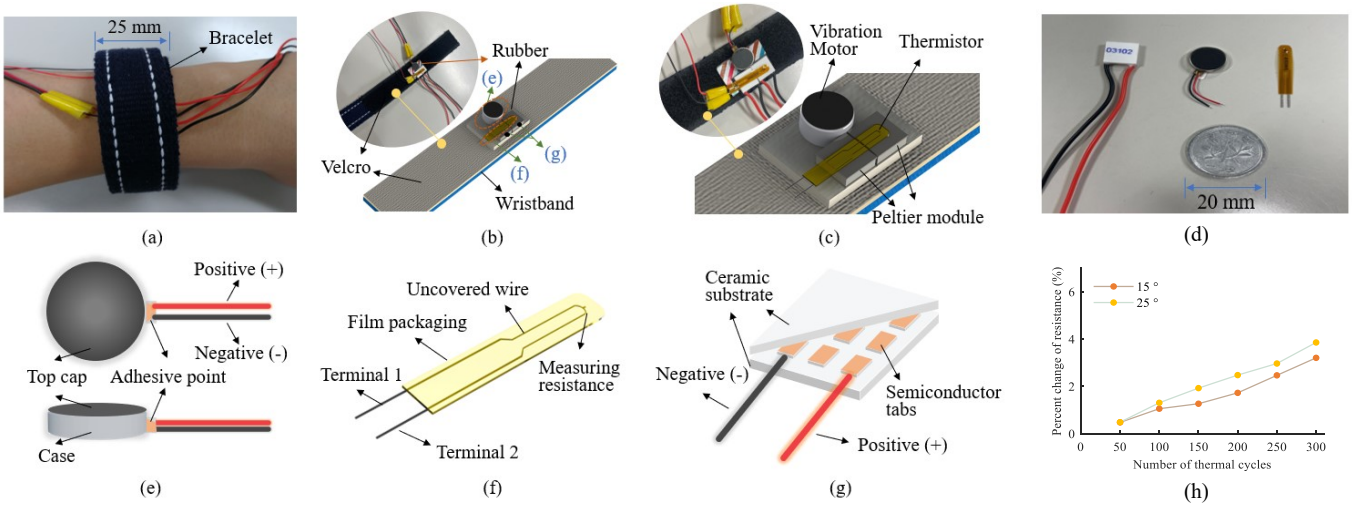

Fig. 3. Prototype of designed WSB and relevant elements: (a) wearing view of WSB; (b) view of internal assembly; (c) view of feedback sensing part; (d) components of feedback sensing part; (e) Mini-type vibration motor; (f) film thermistor; (g) Peltier module; (h) the relationship between the number of thermal cycles and percent change of resistance for Peltier module (reliability performance).

perform safety alert when conducting surgery. A couple of Peltier modules (thermoelectric element, TES1-03102, Hongerda Inc., China) are employed to provide thermal feedback. A piece of rectangular rubber as the bottom support for mounted elements (vibration motor and Peltier modules). The actual views of components are drawn in Fig. 4(d).

Furthermore, a film thermistor (NTC103JT-025, SEMITEC Ltd., Japan) is adopted to measure the temperature between Peltier module and operator's skin in real time. Besides, the proposed WSB is a space-saving and integrated wearable sensing solution for feedback sensing due to all electronic components are encapsulated in a 25 mm wide space.

2) **Leader Manipulator**

The leader manipulator is shown in Fig. 4, which was developed to respect the doctor's original surgical behaviors. From Fig. 4, it was mainly composed of two independent operating units: catheter operating unit (COU) and guidewire operating unit (GOU). It is possible to realize individual operation and simultaneous operation for two instruments. For COU and GOU, they vary in detection methods for both translation and rotation. An integrated photoelectric sensor (MSBJ96, Fujitsu Inc., Japan) is utilized to measure linear movement and rotating movement concurrently for COU as a two-dimensional integration and space-saving detection solution. A laser sensor (LK-500, Keyence Inc., Japan) and an encoder (MES020-2000p, MTL Inc., Japan) are adopted to measure translation motion and rotation motion in GOU, respectively. Structural design for tremor suppression is considered by two ball splines (SLK 006-T2-N5, THK Inc., Taiwan). Additionally, a soft magnetic-actuated haptic interface molded by hydrogel (EcoflexTM, 00-20, Smooth-On Inc., USA) and MR fluid (MRF-122EG, Lord Crop Inc., USA) is proposed to provide a realistic sensation of resistance, which is a tactile information for surgery. The underlying principle of force feedback is to vary fiction between the non-magnetic operating handle and the soft magnetic-actuated structure through controlling density of magnetic field. Benefiting from these designs, the leader manipulator has advantages to operate two instruments, retain natural surgical skills, and offer adjustable force feedback for RES.

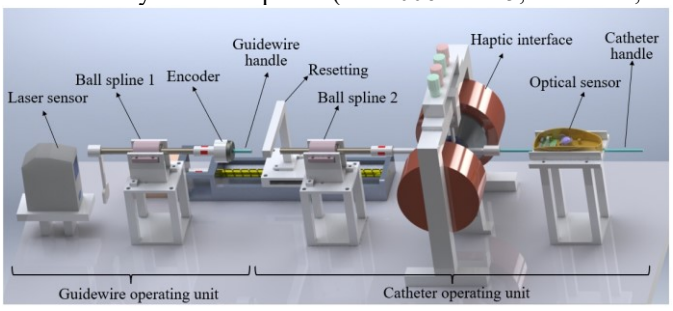

Fig.4. The developed leader manipulator for RES.

3) **Follower Manipulator**

The follower manipulator is designed by previous work of our group [26], as shown in Fig. 5. It was proposed to insert/extract and rotate two kinds of medical instruments for the needs of robot-assisted endovascular surgery, located in patient side. Two independent control units (catheter control unit and guidewire control unit) are presented to delivery linear motion and rotation motion by four stepping motors with a resolution of 0.36 degrees (ASM46AA, ORIENTAL MOTOR, Japan). The synchronous belt is employed to improve the translation movement. Another advantage of follower manipulator is that linear force information of guidewire/catheter can be captured by two load cells (TU-UJ5N, TEAC Inc., Japan, range: -5 N to 5N) when conducting a surgery. Force data not only can demonstrate the interaction condition between robotic system and patient but also can be used to replicate surgical conditions (like force feedback) for surgeons on the leader side.

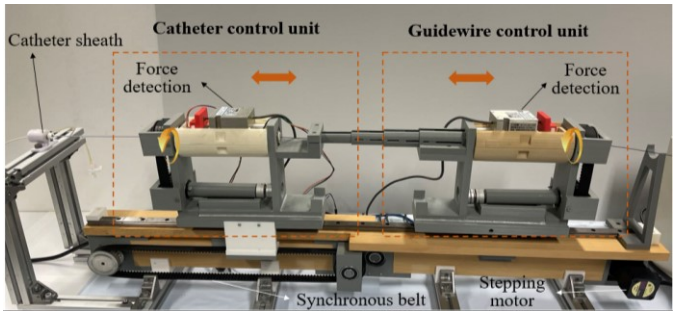

Fig.5. The follower manipulator for RES.

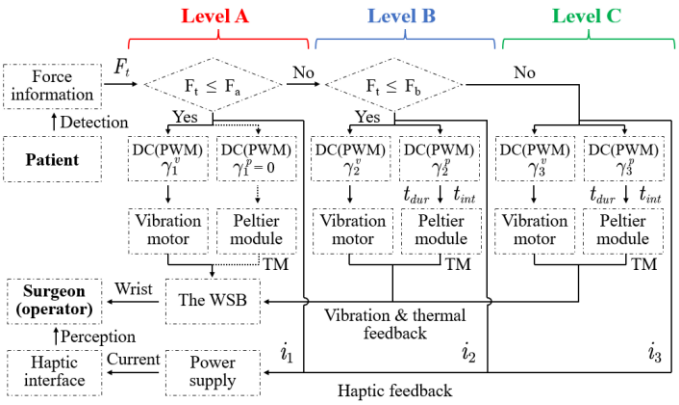

Fig.6. The multilevel control strategy for the feedback sensing system. (DC: duty cycle of PWM; TM: temperature measurement, detected by thermistor)

C.Multilevel Control Strategy of the Sensing System

For the control method of feedback sensing system, it mainly devotes to the tasks of controlling WSB and haptic interface. According to the driving characteristics of vibration motor and Peltier module, a multilevel control strategy was proposed based on different levels of force information detected on follower side, which is depicted in Fig. 6. [27] use force feedback and movement protection mechanism to finish the surgical operations. This study controls multimodal feedback sensing for surgeons through DC(PWM) and supplied current. Refer to [28], the captured total force of follower side can be divided into three levels by two thresholds $F_a = 0.342\ N$ & $F_b = 1.0\ N$, the details of multilevel control strategy are shown in below.

1) Level A (Safe operation): The value of total force is less than F_a. In this case, the DCs (Duty Cycle) of PWM (Pulse Width Modulation) are set to γ_1^v and $\gamma_1^p = 0$, respectively.

2) Level B (Potentially unsafe operation): The value of total force is less than F_b and bigger than F_a. In this condition, the DCs of PWM are set to γ_2^v and γ_2^p, respectively. The duration $t_{dur} = 1.5s$ and the interval $t_{int} = 3.5s$ (refer to [29]) are settled down to ensure a safe operation environment for Peltier module and offer periodic temperature feedback.

3) Level C (Dangerous operation): The value of total force is bigger than F_b. In this situation, the system is able to provide an alarming to remind surgeons as a dangerous operation. The DCs of PWM are set to γ_2^v and γ_2^p, respectively. The parameters of duration t_{dur} and the interval t_{int} are same setting with Level B.

As for the hardware of control, a microcontroller (Arduino UNO, Arduino.cc, Italy) is selected as main control board to realize the proposed control method and measure the surface temperature around the wrist for proposed system. Thanks to the multilevel control strategy, both vibration feedback and thermal feedback embrace three levels sensing as a variable feedback solution. The vibration motor is driven through a dual way Full-Bridge driver module (L298N, VKLSVAN, Japan). Two Peltier modules are controlled by a H-Bridge driver module (L9110 module) due to its micro drive capability and two output groups. In addition, a thermistor was mounted on the heat producing surface of Peltier module to measure the surrounding temperature.

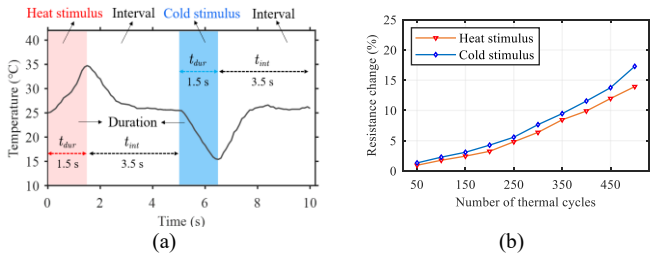

Fig.7. Hardware testing of Peltier module for heat and cold stimulus: (a) change of temperature; (b) change of resistance.

IV. Performance Evaluation

Performance evaluations for three feedback sensing and insertions for the proposed system are carried out to verify the feasibility and repeatability of proposed feedback sensing system in this section. Although laboratory conditions are limited, we strive to ensure the sterility of experimental environment via cleaning devices and improve the compactness of experimental space as much as possible when conducting robot-assisted surgery.

A. Thermal Feedback Sensing

1) **Hardware testing:** to explore the physical property of thermal feedback, two tests are conducted including detecting change of temperature for two stimulus (heat and cold) and measuring change of resistance by numerous thermal cycles (experimental setup is same with Fig. 3(a), no show to avoid repetition). The temperature is captured by the film thermistor. The resistance is measured by a multimeter. Fig. 7 depicts the results of hardware testing of Peltier module for heat and cold stimulus. From Fig. 7(b), it is clear that there is a greater change of resistance under cold stimulus. Hence, heat stimulus is used to provide thermal feedback for operators during this study.

2) **Layout and parameters determination**: Aiming to determine a better layout and suitable parameters for Peltier modules, comparative experiments are conducted for thermal feedback. Fig. 8 shows the layout testing and corresponding thermal sense for Peltier module. Two kinds of layouts (single and double) are utilized to do comparative tests ($30\% - 100\%$ within a fixed increasing step 10%) by five subjects. The starting temperature was set to $33.2\ ℃$ [19]. The index of thermal sense is defined as the cutaneous sensing of subject's wrist (maximum value is set to 10 when the DC for double pieces is provided with 100%). From Fig. 8(c)-(d), the sensing for the layout of double pieces is clearer and easily identifiable for all subjects. Consequently, the layout of double pieces is selected in this work. Moreover, based on the comfort of thermal sensing (heat stimulus) from subjects and the SD (Standard deviation) value in Fig. 8(d), the two parameters (see Fig. 6) for thermal feedback are set to $\gamma_2^P = 70\%$ (slight sense, SD: 0.10 for double pieces) and $\gamma_3^P = 90\%$ (clear sense, SD: 0.17 for double pieces).

3) **Sensing performance and discussion**: to evaluate key information (like resolution, response bandwidth, and repeat accuracy) of thermal feedback, sensing experiments are conducted via microcontroller and designed WSB, which are depicted in Fig. 9. For resolution (see Fig. 9(a)), eight slots of DC ($30\% - 100\%$) are used to measure positive and negative increment with the minimum fixed increment.

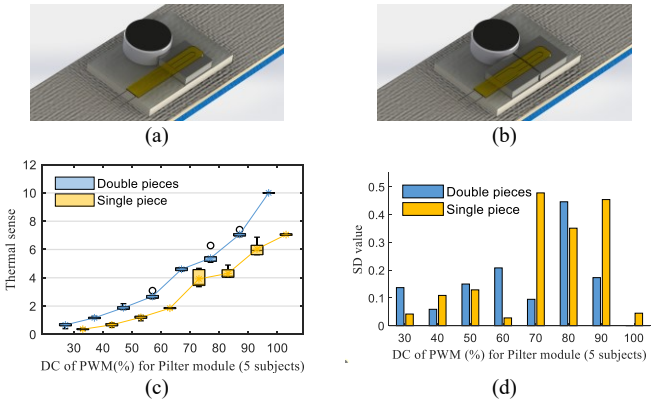

Fig.8. Layout tests and corresponding thermal sense for 5 subjects: (a) layout of single piece; (b) layout of double pieces; (c) results for thermal sense; (d) SD value.

After calculating, thermal feedback achieves average resolution of $0.07\ ℃$ and minimum resolution of $0.01\ ℃$. The response bandwidth of proposed thermal feedback is determined in this part, as illustrated in Fig. 9(b), both frequency increasing and decreasing of input are recorded. The gain of temperature embraces a larger jump (1.092 dB for increasing and 1.688 dB for decreasing) when input frequency changes from 5 Hz to 6 Hz. Hence, the bandwidth for thermal feedback is 5 Hz. As shown in Fig. 9(c)(d), repeat accuracy of thermal feedback is illustrated based on randomized cyclic stimulus and continuous cyclic stimulus. One complete cyclic stimulus consists of heat stimulus and interval (see Fig. 7(a)). For randomized cyclic stimulus, as the increasing of cycle number (30 to 150 times), the value of maximum temperature has a slight decreasing for both two levels ($0.87\ ℃$ for Level B and $1.3\ ℃$ for Level C). Roughly after 35 continuous cycles (running time: 175 s) of continuous stimulus, both two conditions reach to smaller variation range, illustrated in Fig. 9(d) draws the results under cyclic stimulus. Based on above results, the approach of stimulus (heat), layout (double pieces), and key performance (resolution, response bandwidth, and repeat accuracy) of thermal feedback and several are explored and illustrated. Besides, for the realistic sensitivity of surgeon's skin, refer to [21], warm thresholds (like skin's sensitivity) do not decrease any further if the rate at which temperature changes is faster than 0.1 °C/s (the temperature change of our study exceeds by this value, see Fig. 7(a)). Consequently, the wrist's sensitivity for thermal feedback has no big change during the process of thermal feedback. Additionally, the Peltier module shows good durability (The error of temperature is less than 2°C) after more than 1000 cycles. The Arduino runs normally and with rapid response after 48-hour testing. Hence, the thermal feedback can satisfy the requirement (1) listed in Section II.

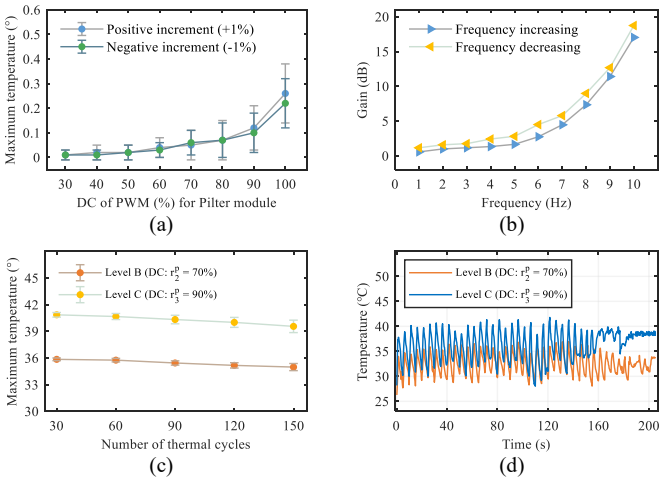

Fig.9. Sensing performance of thermal feedback: (a) resolution; (b) response bandwidth; (c) repeat accuracy for randomized cyclic stimulus; (d) repeat accuracy for continuous cyclic stimulus.

B. Vibration Feedback Sensing

1) **Hardware testing**: To explore the physical property of vibration feedback, tests are conducted based on the vibration motor, drawn in Fig. 10. Firstly, the decibel (loudness) of vibration motor is captured by decibel measurement software under a changing DC range (within a fixed increasing step 4%). Secondly, the current is detected by a multimeter when offering the power to vibration motor. Since the DC is less than 20% for microcontroller, vibration motor does not work. Consequently, the initial DC is set to in this part. It is clear that the decibel of vibration motor reaches to a slow-moving change when the DC is over from Fig. 10(a). The resistance (the change of gradient in Fig. 10(b)) is stable across different levels of supplied voltage (2.6 V-3.6 V).

2) **Parameters determination**: To determine three appropriate parameters for vibration feedback (see Fig. 6), the vibrating senses are recorded from five subjects when applying for a series of DCs of PWM ($20\% - 100\%$ under a fixed increasing step 10%). The results for vibrating sense tests are shown in Fig. 11. The vibrating sense is defined as the sensing of skin of the wrist (maximum value is set to 10 when the DC for vibration motor is offered as 100%). Besides, considering

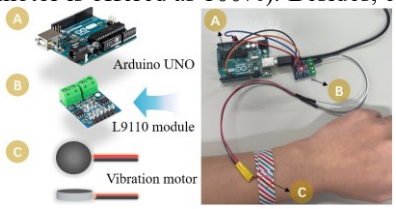

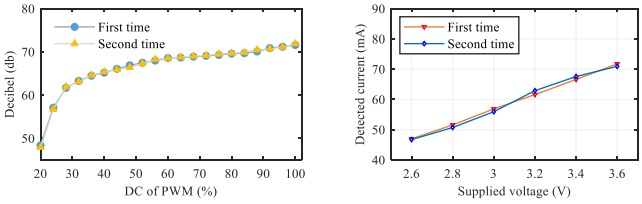

Fig.10. Hardware testing of vibration motor for two times: (a) change of measured decibel; (b) change of detected current.

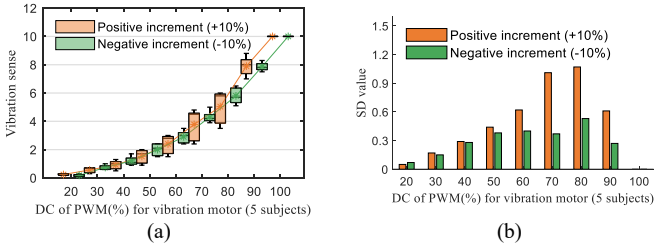

Fig.11. Vibrating sense tests for vibration feedback sensing: (a) results for vibrating sense; (b) SD value.

the comfort of vibration feedback sensing, reduction for prolonged fatigue within vibration feedback, decibel, operation environment, and SD value for positive and negative increment in Fig. 11(b), parameters are determined to be $\gamma_1^v = 30\%$ (SD: 0.17 for PI, 0.15 for NI), $\gamma_2^v = 40\%$ (SD: 0.29 for PI, 0.28 for NI) and $\gamma_3^v = 60\%$ (SD: 0.62 for PI, 0.40 for NI) respectively. Table I depicts the elaborate parameters items.

3) **Sensing performance and discussion:** Similar to the experiments in Section IV-A3, sensing experiments are conducted to demonstrate the sensing performance (surface vibration force, resolution, response bandwidth, and repeat accuracy). Fig. 12 shows the sensing performance of vibration feedback. The experimental setup is shown in Fig. 12(a). The index of surface vibration force (represent sensing intensity) is measured for three conditions (see Fig. 12(b), average values are 0.088 N, 0.097 N, and 0.143 N for DC: $\gamma_1^v, \gamma_2^v, \gamma_3^v$ respectively). For resolution (see Fig. 12(c)), nine slots of DC ($20\% - 100\%$) are used to detect positive and negative (minimum fixed increment: 1%). Vibration feedback obtains average resolution of $0.031\ N$ and minimum resolution of $0.007\ N$. The response bandwidth of thermal feedback is illustrated in Fig. 11(d), both frequency increasing and decreasing of input are calculated. The gain of decibel embraces a larger jump (3.542 dB for increasing and 3.481 dB for decreasing) when the input frequency change from 12 Hz to 15 Hz. Hence, the bandwidth for vibration feedback is 12 Hz. For repeat accuracy of vibration feedback, the decibel (loudness) is measured after the vibration motor was driven by different duration of continuous running under three parameters (30%, 40%, and 60%). The results are shown in Fig. 12(c). As the duration increasing ($20s - 180s$), all of the decibels for three conditions have a slight fall (0.17, 0.65, 0.46 for three conditions, respectively). Based on these results, the proposed vibration feedback can satisfy the requirement (2) listed in Section II.

C. Force Feedback Sensing

The soft magnetic-actuated haptic interface has been proposed in our study [20] as a new solution for force feedback.

TABLE I
PARAMETERS ITEMS PROPOSED IN THIS WORK

Parameters Items	Value	Parameters Items	Value
Threshold F_a	0.342 N	DC γ_1^p	0%
Threshold F_b	1.0 N	DC γ_2^p	70%
DC γ_1^v	30%	DC γ_3^p	90%
DC γ_2^v	40%	Duration t_{dur}	1.5 s
DC γ_3^v	60%	Interval t_{int}	3.5 s

The calibration experiments have illustrated the co-relationship between the input (current) and the output (tactile force). In this part, we explored the sensing performance to demonstrate feasibility and efficacy of force feedback.

1) **Sensing performance**: to evaluate key performance (like accuracy, resolution, response bandwidth, and repeat accuracy), sensing experiments are conducted, illustrated in Fig. 13. The experimental setup is shown in Fig. 13 (a) including force detection and force generation. The accuracy of haptic interface is shown in Fig. 13(b). There are tiny delays occur in running time. So, it is better to calculate the error artificially instead of subtracting directly. The maximum error is 0.09 N, and the maximum relative error is 15.89%. For resolution (see Fig. 13(c)), eight slots of current are used to measure positive and negative increment ($0.3V - 2.4V$ within fixed increment: $0.3V$). It obtains average resolution of $0.053N$ and minimum resolution of $0.01N$. The response bandwidth of force feedback is illustrated in Fig. 13(d). The gain of force embraces a larger jump (2.166 dB for increasing and 2.263 dB for decreasing) when the input frequency changes from 18 Hz to 21 Hz. Hence, the bandwidth for force feedback is 18 Hz. For repeat accuracy of force feedback, three kinds of supplied current (0.9A, 1.5A, 2.1A) are used to do the tests of continuous running. The results of repeat accuracy are shown in Fig. 13(e). With the duration increasing ($20s - 180s$), all tactile values for three conditions have a slight fall (0.027N, 0.018N, 0.032N for supplied current: 0.9A, 1.5A, 2.1A, respectively).

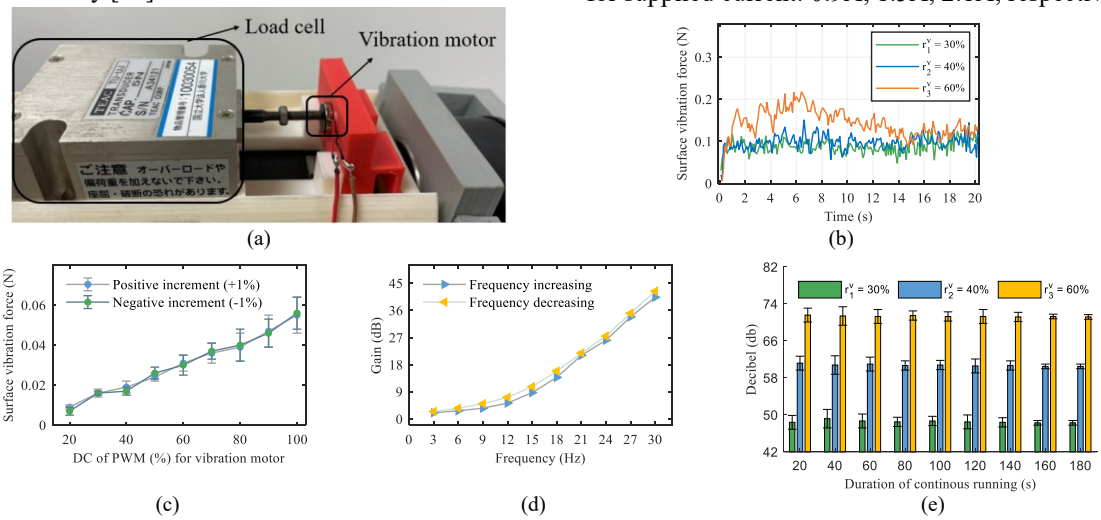

Fig.12. Sensing performance of vibration feedback: (a) experimental setup; (b)surface vibration force. (c) resolution; (d) response bandwidth; (e) repeat accuracy.

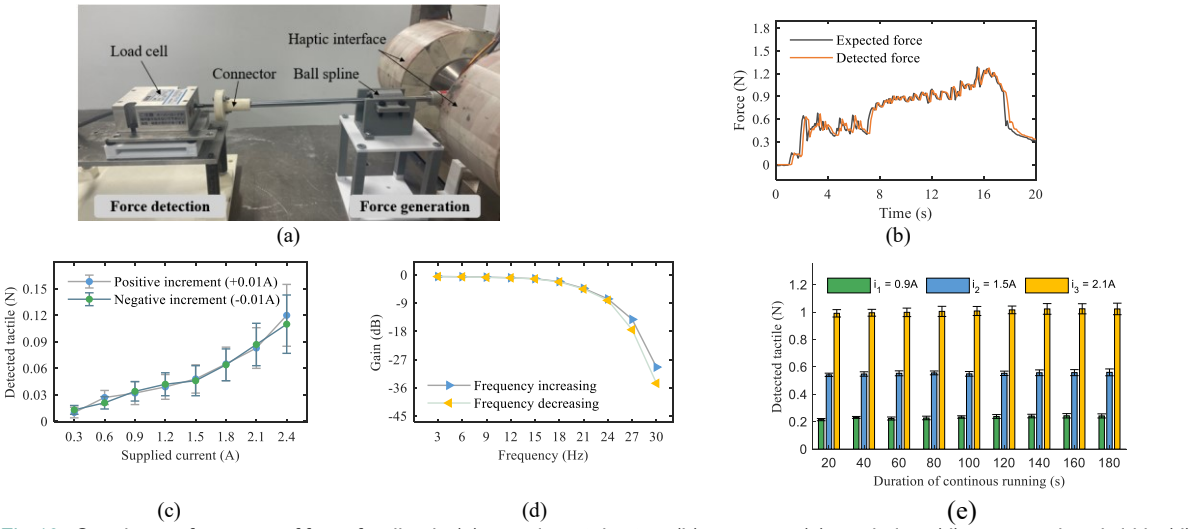

Fig.13. Sensing performance of force feedback: (a) experimental setup; (b) accuracy; (c) resolution; (d) response bandwidth; (d) repeat accuracy for continuous running.

2) **Discussion**: For force feedback, from Fig. 13(b), there are tiny delays (the maximum delay is 300 ms) existing, mainly due to the specific hysteresis of haptic interface (two coils) and could be reduced by fitting hysteretic curve [21]. In [30], force resolution is proposed as minimum incremental value. Hence, the resolution of force feedback is $0.01N$. Based on these results of Section IV-C, the proposed force feedback can satisfy the requirement (3) listed in Section II. In addition, it would be helpful and instructive to offer reliable, repeatable, and response-fast force feedback as a soft solution.

D. In Vitro Experiments

1) **Insertion performance**: To verify whether the vascular robotic system with proposed multimodal sensing feedback can perform automatically and test the experimental performance with the multilevel control strategy, in vitro experiments were carried out through an endovascular evaluator (EVE, Fain-Biomedical Inc., Japan). The in vitro setup is shown in Fig. 14 including leader side and follower side. The catheter employed in this work is a 4 Fr catheter ($1Fr \approx 0.333mm$, Terumo Co., Japan). The fluid control unit is to generate circulating blood flow for EVE modal. The temperature of stimulated blood is $25.4\ ^{\circ}C$. A medial sheath is used to support the instruments and retain surgical environment. The force is detected by load cell and amplified by a strain amplifier (SA-570ST, TEAC Inc., Japan). To make clear comparisons, three kinds of procedures were conducted for descending aorta, aorta arch, and left common carotid artery. Fig. 15 depicted comparison results of in vitro experiments for three procedures. The force for insertion of descending aorta is detected for different conditions within MF maximum force within MF is 0.981 N (less than F_b, operations belong to level A and level B), the maximum force within TF is 0.938 N, and the maximum temperature of thermal feedback is $35.68\ ^{\circ}C$. Meanwhile, the changes of DC(PWM) for both Peltier module and vibration motor are recorded. Fig. 15(b) depicts the experimental performance for aorta arch with the maximum force of 1.805 N within MF (over F_b, operations include level A, level B, and level C). Correspondingly, the maximum force within TF is 2.210 N. The specific shape of aorta arch makes the value of

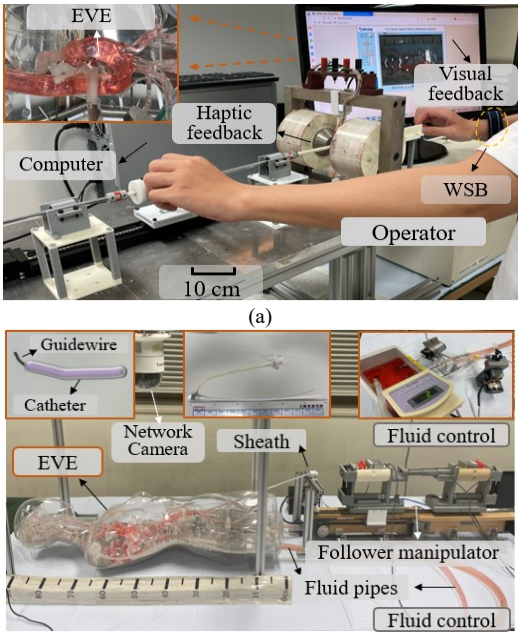

Fig.14. Setup for in vitro experiment: (a) leader side; (b) follower side.

detected force higher. The maximum temperature of WSB is $39.78\ ^{\circ}C$ for this case. The experimental results for left common carotid artery are exhibited in Fig. 15(c) with a maximum force of 2.513 N within MF (above F_b , operations are classified to level A, level B, and level C). The maximum force within TF is 2.792 N. The reason mainly is that the insertion access becomes longer and more complex after entering the right branched vascular. The maximum temperature of WSB is $40.56\ ^{\circ}C$. In addition, the minimum fallback temperature of heat cycle shows a slow upward trend and stabilize to $35\ ^{\circ}C$ via numerous heat cycles. Under the same experimental conditions (eg., parameter setting, force detection, temperature measurement and experimental setup), five subjects (college students from Kagawa University, age: 20-28, in good condition) successfully perform the EVE experiments for three procedures, which are shown in Table II, it can demonstrate feasibility and repeatability of proposed

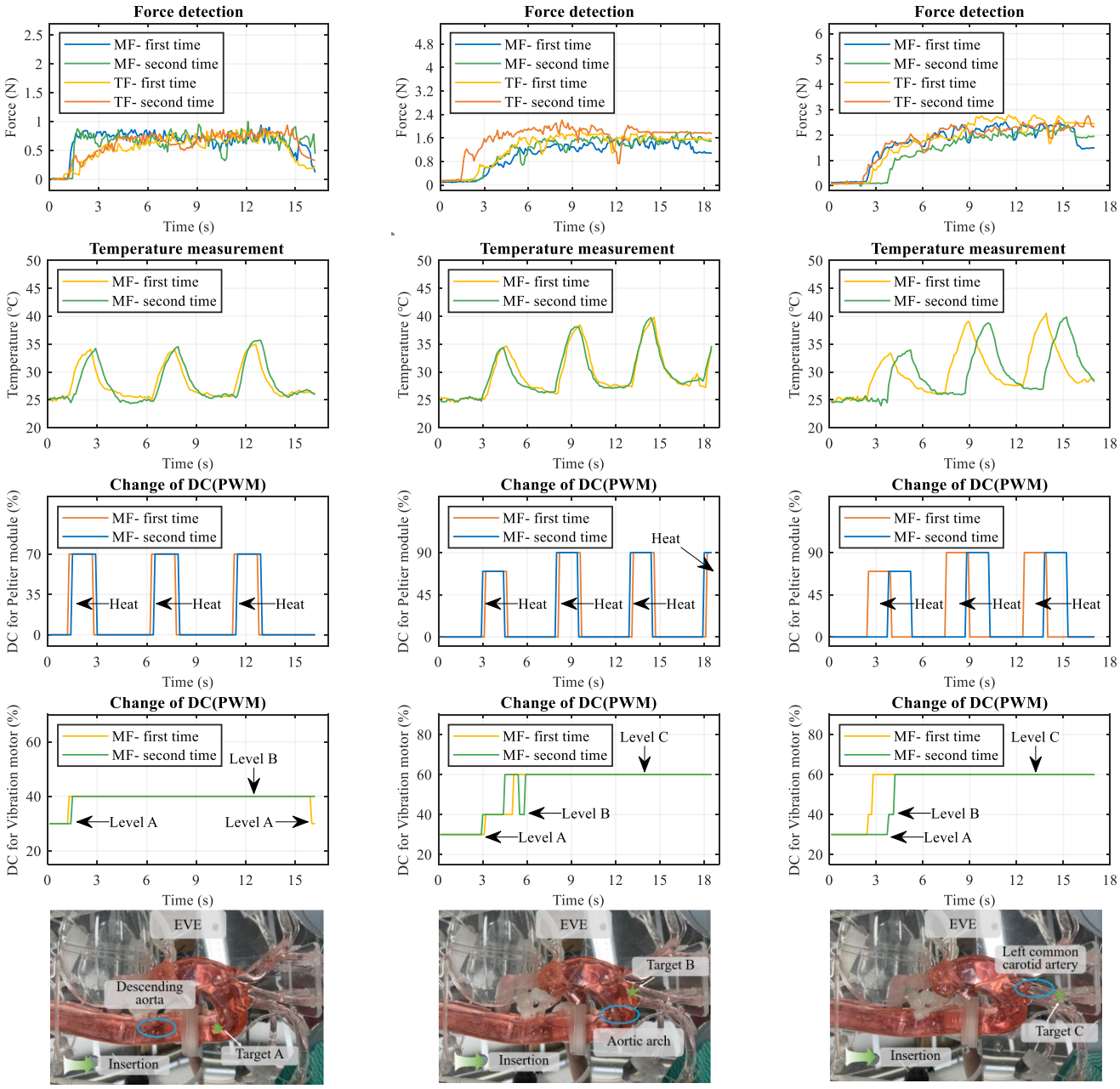

Fig.15. Comparison results of in vitro experiments under three procedures: (a) descending aorta; (b) aortic arch; (c) left common carotid artery. (MF: Multimodal feedback, TF: Traditional feedback)

multimodal feedback sensing system as an immersive solution. The maximum values of force within MF for three procedures are 0.939 N, 1.866 N, and 2.614 N, respectively. The maximum values of temperature for three procedures are $36.37\,℃$, $40.17\,℃$, and $40.56\,℃$. In addition, the comparison results for maximum force and completion time are shown in Fig. 16. The maximum forces are 0.883 N, 2.132 N, and 2.789 N within TF. The force data moves to 0.939 N, 1.866 N, and 2.614 N within MF. Similarly, the average completion times are 19.0 s, 28.6 s, and 35.0 s within TF, and the values move to 19.4 s, 33.2 s, and 42.4 s within MF, respectively.

2) **Discussion**: We discuss the results of in vitro experiments based on both TF and MF experiments to compare relative performance. For force detection, the varying trends for both TF and MF are embracing a rise from procedure 1 to procedure 3 (see force detection in Fig. 15 and Fig. 16(a)(b)). It occurs mainly due to the complexity for different vessels and insertion paths. From Fig. 16, for procedure 1, the maximum forces (0.898 N and 0.939 N) and the average completion times (19.0 s and 19.4 s) are almost same between the conditions within TF and MF. This happened because the vessel of procedure 1 is pretty flat and thick, both operations for TF and MF belong to potentially unsafe operations (Level B). For procedure 2, the maximum forces are 1.866 N within TF and 1.713 N within MF, respectively. In this case, the proposed MF provided a safer operation for VIS based on the immersive sensing. Additionally, operations within MF result in average completion times (28.6 s for TF and 33.2 s for MF) has a slight growing. Similarly, for

TABLE II
INSERTION PERFORMANCE OF FIVE SUBJECTS IN DIFFERENT PROCEDURES (WITHIN MF)

Items	Procedure 1: Descending Aorta				Procedure 2: Aortic Arch				Procedure 3: Left Common Carotid Artery			
	Average Force (N)	Maximum Force (N)	Average Temperature (℃)	Maximum Temperature (℃)	Average Force (N)	Maximum Force (N)	Average Temperature (℃)	Maximum Temperature (℃)	Average Force (N)	Maximum Force (N)	Average Temperature (℃)	Maximum Temperature (℃)
Subject 1	0.652	0.939	28.00	34.98	1.049	1.582	29.67	39.78	1.706	2.513	30.08	40.56
Subject 2	0.637	0.882	27.93	35.56	1.192	1.807	29.58	39.64	1.435	2.408	29.63	39.95
Subject 3	0.618	0.855	28.86	36.37	0.981	1.514	29.47	39.08	1.642	2.447	29.91	40.08
Subject 4	0.545	0.835	28.46	36.08	1.299	1.866	30.28	40.17	1.817	2.544	29.82	40.26
Subject 5	0.548	0.881	29.00	36.02	1.274	1.800	29.86	39.51	1.674	2.614	30.11	40.43

procedure 3 within a more complex and thinner vessel, the maximum forces are 2.789 N within TF and 2.614 N within MF, respectively. The average completion times (35.0 s for TF and 42.4 s for MF) has a slight growing. It also demonstrates that proposed MF offers safe operations for complex surgical environments. Furthermore, from insertion performance of five subjects (see Table II), the values of average force, maximum force, average temperature, and maximum temperature for three procedures clearly verify the feasibility and repeatability for the robotic system with proposed multimodal feedback sensing. By this mean, our effort can successfully reflect the conditions for different lesions and provide suitable feedback sensing to ensure continuous safe operation. Furthermore, a one-way Analysis of Variance (ANOVA) was conducted for statistical tests (p-value), as TABLE III shown. The p-value (less than 0.05) indicates that the force feedback and thermal feedback are effective and significant.

For further consideration, benefiting from good portability (see Fig. 3) and repeatability (see repeat accuracy, Fig. 9, Fig. 12, and Fig. 13), easy control (see Fig. 6), and insertion performance (see Section IV-D), the proposed multimodal feedback sensing has potential use value in other engineering systems or medical applications that requires feedback sensing to ensure safe operations. Even if we follow the research approach of multimodal feedback sensing, numerous pattens can be reconstructed, like electrical stimulation, light stimulation, proper acupuncture could be combined to provide more immersive feedback sensing for robotic engineering scenarios. The commercial RES system (e.g., CorPath GRX) has advantages in sterilization and operating room integration and even develops remote communication and navigation systems. Compared with CorPath GRX, our work focuses on the explorations for multimodal feedback sensing to offer immersive feedback and safe operation environment.

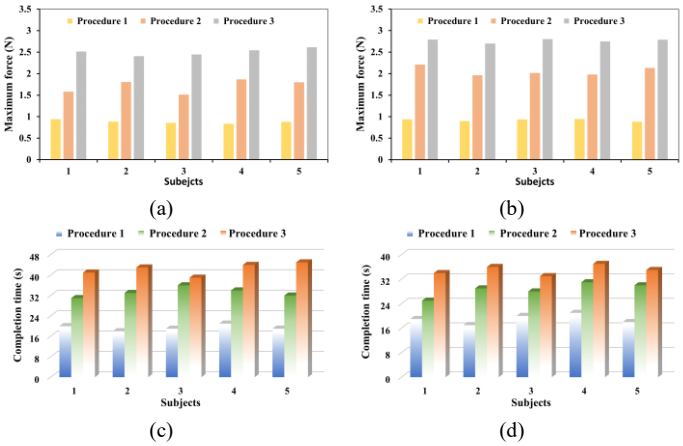

Fig.16. Comparison results for maximum force and completion time under three procedures: (a) maximum force within MF; (b) maximum force within TF; (c) completion time within MF; (d) completion time within TF.

However, a few limitations existed in this work including the difficulty to ensure the dynamic accuracy for long-time feedback procedure and the concern to improve the issue of time delay. The average value of time delay for thermal feedback, vibration feedback, and haptic feedback are 0.25 s, 0.11 s, and 0.17 s, respectively. These observations might be enhanced by employing Pelletier modules and vibration motors with higher accuracy and sensitivity, even by adopting better communication technology like 5G. Meanwhile, clinical evaluations and verifications are not performed due to constraints of the current laboratory environment. These limitations might be improved through building collaborations with hospitals. In addition, through the latest 5G wireless communication technology [31], it can embrace a huge possibility for remote and mobile operation for surgeons.

V. CONCLUSION

In this work, a novel multimodal feedback sensing system for RES was developed and its performance was evaluated by both exploring experiments and vitro experiments. In summary, there are three core contributions in this work including (1) a multimodal feedback sensing system integrated with four kinds of feedback based on the integrated WSB, haptic interface, and visual window; (2) a multimodal control strategy based on four kinds of feedbacks to build an immersive feedback sensing experience for surgeons, which is beneficial to automatically distinguish different surgical conditions and guide safe operation procedures during RES; (3) performance evaluations demonstrate that proposed feedback system could satisfy clinical requirements of leader-follower operation and have potential to use in other robotics. Moreover, this work will play a greater role in engineering for RES to improve operation transparency and safety, even can be used to train more

TABLE III
STATISTICAL TESTS FOR SUBJECTS

Items	p-value	
	Force (N)	Temperature (℃)
Subject 1	0.0065	0.0157
Subject 2	0.0117	0.0132
Subject 3	0.0098	0.0998
Subject 4	0.0073	0.0183
Subject 5	0.0086	0.0206

inexperienced doctors with low cost and short training period. For future work, more intelligent feedback sensors, communication technology, and augmented reality might be integrated to optimize the experience of human-robot interaction and realize deep immersion for RES.

REFERENCES

[1] X. Li et al., "Soft Magnetic-Actuation-Based Haptic Interface for a Robot-Assisted Vascular Interventional System: A Feasibility Study," *IEEE Sensors J.*, vol. 24, no. 1, pp. 710-721, 2024.

[2] Y. Yan, S. Guo, B. Shen., et al., "5-DOF Microcoil Positioning System Utilizing Single-Axis Electromagnetic Transmitter," *IEEE/ASME Trans. Mechatronic*, Doi: 10.1109/TMECH.2025.3554246, 2025.

[3] C. Lyu, S. Guo, Y. Yan., et al., "Deep Learning-based Force Sensing Method for a Flexible Endovascular Surgery Robot," *IEEE Transactions on Instrumentation and Measurement*, vol. 73, 7503910, Doi: 10.1109/TIM.2024.3381290, 2024.

[4] M. Tiwana, S. Redmond, and N. Lovell, "A review of tactile sensing technologies with applications in biomedical engineering," *Sens. Actuator A Phys.*, vol. 179, pp. 17-31, Jun. 2012.

[5] G. Gu, N. Zhang, H. Xu et al., "A soft neuroprosthetic hand providing simultaneous myoelectric control and tactile feedback," *Nat. Biomed. Eng.*, vol. 7, pp. 589-598, Aug. 2023.

[6] A. Hooshiar, A. Payami, J. Dargahi, and S. Najarian, "Magnetostriction-based force feedback for robot-assisted cardiovascular surgery using smart magnetorheological elastomers," *Mech. Syst. Signal Processing*, vol 161, p. 107981, Dec. 2021.

[7] D. Kundrat et al., "An MR-Safe endovascular robotic platform: design, control, and ex-vivo evaluation," *IEEE Trans. Biomed. Eng.*, vol. 68, no. 10, pp. 31974-31982, Oct. 2021.

[8] Y. Yan, S. Guo, C. Lyu, et al., "SEA-based Humanoid Finger-functional Parallel Gripper with Two Actuators: PG2 Gripper," *IEEE Trans. Instrum. Meas.*, vol. 72, Dec. 2022, doi: 10.1109/TIM.2022.3229695.

[9] S. Guo, Y. Song, X. Yin, et al., "A Novel Robot-Assisted Endovascular Catheterization System with Haptic Force Feedback," *IEEE Trans. Robot.*, vol. 35, no. 3, pp. 685-696, Jun. 2019.

[10] A. K. Bastola, and M. Hossain, "A review on magneto-mechanical characterizations of magnetorheological elastomers," *Compos. Part B: Eng.*, vol. 200, p. 108348, Nov. 2020.

[11] X. Li, S. Guo et al., "An Endovascular Catheterization Robotic System Using Collaborative Operation with Magnetically Controlled Haptic Force Feedback," Micromachines, vol. 13, no. 4, 505, 2022.

[12] A. Hooshiar et al., "Development and assessment of a stiffness display system for minimally invasive surgery based on smart magneto-rheological elastomers," *Syst. Signal Processing.*, vol. 108, Mar. 2020.

[13] M. Rehan, M. M. Saleem et al., "A Soft Multi-Axis High Force Range Magnetic Tactile Sensor for Force Feedback in Robotic Surgical Systems," *Sensors*, vol. 22, no. 9, May 2022.

[14] P. E. Dupont, B. J. Nelson, M. Goldfarb et al., "A decade retrospective of medical robotics research from 2010 to 2020," *Science Robotics*, vol. 6, no. 60, Nov. 2021.

[15] Y. Yan, H. Wang, H. Yu, F. Wang, J. Fang, J. Niu, and S. Guo, "Machine Learning-based Surgical State Perception and Collaborative Control for a Vascular Interventional Robot," *IEEE Sensors J.*, DOI. 10.1109/JSEN.2022.3154921, 2022.

[16] E. Pezent et al., "Design, Control, and Psychophysics of Tasbi: A Force-Controlled Multimodal Haptic Bracelet," *IEEE Trans. Robot.*, vol. 38, no. 5, pp. 2962-2978, Oct. 2022.

[17] K. Y. Chun et al., "A Wearable All-Gel Multimodal Cutaneous Sensor Enabling Simultaneous Single-Site Monitoring of Cardiac-Related Biophysical Signals," *Advanced materials*, vol 34, no. 16, Feb. 2022.

[18] S. Chun, J. Kim, Y. Yoo et al., "An artificial neural tactile sensing system," *Nature Electronics*, no. 4, pp. 429-438, Jun. 2021.

[19] R. L. Peiris et al., "ThermalBracelet: Exploring Thermal Force feedback Around the Wrist," in Proc. 2019 CHI Conference on Human Factors in Computing Systems, no. 170, Glasgow Scotland, UK, May. 2019, pp. 1-11.

[20] X. Li et al., "A Bimodal Detection-based Tremor Suppression System for Vascular Interventional Surgery Robots," *IEEE Trans. Instrum. Meas.*, vol. 71, 4009612, Oct. 2022, doi: 10.1109/TIM.2022.3216367.

[21] X. BAO et al., "Haptic Interface With Force and Torque Feedback for Robot-Assisted Endovascular Catheterization," *IEEE/ASME Trans. Mechatronic*, vol. 29, no. 2, pp. 1111-1125, Jul. 2023.

[22] C. Joseph et al., "Temperature sensitivity of the body surface over the life span," *Somatosens. Mot. Res.*, vol. 15, no. 1, p. 13-28, 1998.

[23] F. Liao et al., "Ultrasensitive Flexible Temperature-Mechanical Dual-Parameter Sensor Based on Vanadium Dioxide Films," *IEEE Electron Device Lett.*, vol. 38, no. 18, pp. 1128-1131, Aug. 2017.

[24] L. Wei et al., "An FBG-Sensing Two-Dimensional Vibration Sensor Based on Multi-Axis Flexure Hinge," *IEEE Sensors J.*, vol. 19, no. 10, pp. 3698-3710, May. 2019.

[25] J. An, D.S. Kwon, "Modeling of a Magnetorheological Actuator Including Magnetic Hysteresis," *J. Intell Mater. Syst. Struct.*, vol. 14, no. 9, Sep. 2003.

[26] X. Jin et al., "Development of a Tactile Sensing Robot-Assisted System for Vascular Interventional Surgery," *IEEE Sensors J.*, vol. 21, no. 10, pp. 12284-12294, May. 2021.

[27] X. Bao et al., "Multilevel operation strategy of a vascular interventional robot system for surgical safety in teleoperation," *IEEE Trans. Robot.*, vol. 38, no. 4, pp. 2238-2250, Aug. 2022.

[28] X. Jin et al., "Active Suppression Method of Dangerous Behaviors for Robot-Assisted Vascular Interventional Surgery," *IEEE Trans. Instrum. Meas.*, vol. 71, Apr. 2022, doi: 10.1109/TIM.2022.3170997.

[29] M. Nakatani et al., "A Novel Multimodal Tactile Module that Can Provide Vibro-Thermal Feedback," *Haptic Interaction,* vol. 432, pp. 437-443, Singapore, Jul. 2017.

[30] E. Samur, "Performance evaluation based on psychophysical tests," *in Performance Metrics for Haptic Interfaces. London, U.K.: Springer-Verlag*, pp. 81–106, 2012.

[31] E. Dahlman et al., "What is 5G?," *5G/5G-Advanced.*, Doi: 10.1016/b978-0-443-13173-8.00008-6, pp. 1-5, 2024.

Xinming Li (Member, IEEE) got the Ph.D. degree in intelligent mechanical systems engineering with the Graduate School of Engineering, Kagawa University, Japan, in 2024. He is currently a Lecturer with the School of Intelligent Manufacturing, Guangzhou Maritime University, China.
His research includes robotic-assisted VIS, safety operation, and feedback sensing.

Shuxiang Guo (Fellow, IEEE) is currently a Chair Professor with the Department of Electronic and Electrical Engineering, Southern University of Science and Technology, Shenzhen, China. He is also a Chair Professor with the Key Laboratory of Convergence System and Healthcare Technology Medical Engineering, Beijing Institute of Technology, Beijing, China.
Prof. Guo has a fellowship of The Engineering Academy of Japan.

Masahiko Kawanishi received the B.S. degree from the Faculty of Medicine of Kagawa Medical University, Kagawa, Japan, in 1993.
He is currently a Lecturer with the Faculty of Medicine, Kagawa University, Japan.

Keisuke Suzuki is currently a Professor with the Graduate School of Engineering, Kagawa University, Takamatsu, Japan.
Prof. Suzuki is a Fellow of JSAE. He is also the chairman of the Advanced Simulator Study Group organized by JSME.